Climate Dynamics
https://doi.org/10.1007/s00382-019-04881-3

Understanding the interannual variations of the zonal mean Indian summer monsoon seasonal rainfall

Sarvesh Dubey[1,2] · **Vasubandhu Misra**[2,3,4]

Received: 4 January 2019 / Accepted: 25 June 2019

Abstract
In this study, we seek to understand the variations of the zonal mean Indian summer monsoon (ISM). It is observed that the zonal mean precipitation anomalies explain about 20–30% of the total seasonal precipitation of the ISM. Additionally, we also show that the interannual anomalies of the ISM, at least for some of the most extreme seasons display significant zonal symmetry. Therefore, understanding the interannual variations of the zonal mean precipitation is quite relevant. Furthermore, the reduced and simplified dimensionality of the zonally symmetric framework is an additional attraction. Our study shows that the zonal mean precipitation anomalies of the ISM are significantly correlated with the corresponding anomalies of the vertically integrated moist static energy (H) at interannual scales. The forcing terms of the tendency of the zonal mean H of the ISM is dominated by the meridional flux of H by the Hadley cell followed by comparably smaller, yet, significant forcing terms of transverse boundary and vertical fluxes of H. We find that the individual correlations of the zonal mean precipitation anomalies of the ISM with each of these dominant terms of H are comparably weak in the core latitudes of the ISM. But some of the relatively weaker forcing terms of H like the radiative heating and the diffusion of the enthalpy fluxes display a very strong relationship with the corresponding zonal mean precipitation anomalies. These results suggest that although the description of the regional Hadley cell offers a heuristic model to describe the ISM variation, it belies the intricacies of the forcing terms that maintain it. Our study suggests that the challenge of the ISM seasonal rainfall anomaly prediction even in a reduced dimensional space of a zonally symmetric framework requires all the forcing terms of H with reasonable fidelity, irrespective of their contribution to the variations of H.

1 Introduction

Early theories of atmospheric general circulation started with the 2-D zonally symmetric framework following Hadley (1735). Hadley (1735) came up with the concept of the mean meridional circulation that bears his name which consists of rising motions in the lower latitudes and sinking motion in the higher latitudes with equatorward flow at low levels and poleward flow at upper levels. This meridional Hadley circulation is now well established from theory (Palmen 1963; Riehl 1963; Lorenz 1967; Held and Hou 1980) and verified from a growing density of observations over time (Tucker 1959; Palmen and Vuorela 1963; Vuorela and Tuominen 1964; Oort and Rasmusson 1970; Oort and Yienger 1996). To this day this fundamental concept of the atmospheric general circulation continues to be used to validate models (Johanson and Fu 2009), reanalysis (Waliser et al. 1999), and understand manifestations of a future evolving climate (Lu et al. 2007; Waugh et al. 2015).

A regional Hadley circulation is invoked to understand the variations of the Indian Summer Monsoon (ISM; Schulmann 1973; Joseph 1978; Goswami 1994; Goswami et al. 1999; Slingo and Annamalai 2000). This regional Hadley cell responds to the ISM rainfall that produces the diabatic heating maximized around the latitude band of 15°N–20°N (Goswami et al. 1999). In contrast to the prevalent global Hadley circulation that has its ascending branch anchored around 5°N, Schulmann (1973) noted that the asymmetric heat source of the ISM drives a regional

✉ Sarvesh Dubey
skdubey@cas.iitd.ac.in

1 Centre for Atmospheric Sciences, Indian Institute of Technology Delhi, Hauz Khas, New Delhi 110016, India

2 Department of Earth, Ocean and Atmospheric Science, Florida State University, Tallahassee, FL, USA

3 Center for Ocean-Atmospheric Prediction Studies, Florida State University, Tallahassee, FL, USA

4 Florida Climate Institute, Florida State University, Tallahassee, FL, USA

Published online: 05 July 2019

Hadley cell over the Indian Ocean with its ascending branch around 15°N–20°N and its descending branch over the equator and further south in the southern hemisphere subtropics. In fact, Slingo and Annamalai (2000) suggest that this regional Hadley cell is far more responsive to interannual variations of the ISM than the global Hadley cell. Many of the earlier studies view the ISM as a superposition of this regional, lateral Hadley cell with the transverse, planetary-scale Walker circulation (Goswami 1994; Webster et al. 1998; Krishnamurthy and Goswami 2000).

In terms of understanding the interannual variations of the ISM, several indices have been developed to capture the variations in the associated circulations (Webster and Yang 1992; Goswami et al. 1999). For example, Goswami et al. (1999) find that a strong (weak) regional Hadley and weak (strong) Walker circulation is associated with strong (weak) ISM seasonal rainfall anomaly. Krishnamurthy and Shukla (2000) illuminate on the various alternative paradigms for explaining the interannual variations of the ISM: one in which the ISM seasonal rainfall anomaly responds to external forcing (e.g. ENSO variations), another in which the ISM seasonal rainfall anomaly is a result of internal (chaotic) variations of the ISM itself or ISM seasonal rainfall anomaly is a combination of the external forcing and internal variability. A conclusive resolution of these paradigms has been somewhat illusive because of the potential feedbacks between the internal and the external variability components. Nonetheless, it is tempting to resolve this issue as it has strong implications on the seasonal predictability of the ISM. In the recent past, however, there has been a spurt of studies that indicate useful seasonal predictability of the ISM using SST anomalies (Wang et al. 2015; Li and Wang 2016; Nigam et al. 2018).

The column-integrated moist static energy (H) is an essential ingredient for tropical convection (Neelin and Held 1987; Raymond 2000; Yasunaga and Mapes 2012; Inoue and Back 2015). It is found that the evolution of the H evolves with the precipitation anomalies in the tropics (Inoue and Back 2015). This is primarily on account of the conservation of H for moist processes with temperature and geopotential anomalies being small in the tropics (Bretherton and Smolarkiewicz 1989; Sobel and Bretherton 2000). The time tendency equation of H following Yanai et al. (1973) is:

$$\overline{\frac{\partial H}{\partial t}} = -\int_{p_{top}}^{p_{bot}} \nabla \cdot \overline{\vec{V}(h)}\frac{dp}{g} - \int_{p_{top}}^{p_{bot}} \frac{\partial \overline{\omega(h)}}{\partial p}\frac{dp}{g} + \overline{Q_R}, \tag{1}$$

where $H = \int_{p_{top}}^{p_{bot}} h\frac{dp}{g}$, h is the moist static energy at a given pressure level, $\vec{V}$ is the horizontal velocity, and $\omega = \frac{Dp}{Dt}$ is pressure velocity. Q_R is the vertically integrated radiative heating rate. p_{bot}, p_{top} are pressure levels at the bottom and top of the atmosphere respectively. The overbar represents seasonal mean.

Now, for a zonally symmetric framework and seasonal mean, we can rewrite Eq. (1) as:

$$\overline{\frac{\partial [H]}{\partial t}} = -\int_{p_{top}}^{p_{bot}} \left(\frac{\partial \overline{[hv]}}{\partial y}\right)\frac{dp}{g} - \int_{p_{top}}^{p_{bot}} \frac{\partial \overline{[\omega][h]}}{\partial p}\frac{dp}{g} + \overline{[Q_R]} + \overline{[EF]}, \tag{2}$$

where the square brackets represent global zonal mean and EF stands for the surface enthalpy fluxes. The zonal fluxes in Eq. (2) identically vanishes in the case of zonal mean taken around the globe due to the cyclic boundary condition. However, over a limited domain a non-zero east–west (transverse) boundary flux (B_Q) also exists. Therefore, Eq. (2) may be rewritten for a regional domain that is inclusive of the ISM as:

$$\overline{\frac{\partial [H]}{\partial t}} = -\int_{p_{top}}^{p_{bot}} \left(\frac{\partial \overline{[hv]}}{\partial y}\right)\frac{dp}{g} - \int_{p_{top}}^{p_{bot}} \frac{\partial \overline{[\omega][h]}}{\partial p}\frac{dp}{g} + \overline{[Q_R]} + \overline{[EF]} - \overline{B_Q}, \tag{3}$$

where square brackets in Eq. (3) refer to a zonal mean within the regional longitudes (in our case 60°E–100°E). In this study, we will study the individual terms of Eq. (3) to understand the variations of the zonal mean H. We will further try to understand the relationship of the zonal mean precipitation anomalies of the ISM with the corresponding zonal mean H. In the following section we describe the methodology and the datasets used for the study. The results are discussed in Sect. 3 and concluding remarks are provided in Sect. 4.

2 Methodology and datasets

The first term on the right-hand side of Eq. (3) can be further broken down as:

$$\frac{\partial}{\partial y}\int_{p_{top}}^{p_{bot}} \left[\overline{hv}\right]\frac{dp}{g} = \frac{\partial}{\partial y}\int_{p_{top}}^{p_{bot}} \left[\overline{h}\right]\left[\overline{v}\right]\frac{dp}{g} + \frac{\partial}{\partial y}\int_{p_{top}}^{p_{bot}} \overline{[h'][v']}\frac{dp}{g} + \frac{\partial}{\partial y}\int_{p_{top}}^{p_{bot}} \left[\overline{h^* v^*}\right]\frac{dp}{g}, \tag{4a}$$

where the individual terms of Eq. (4a) can be expressed in discrete form as:

$$\left[\overline{hv}\right] = \frac{1}{N}\sum_{i=1}^{N}[h_i v_i], \tag{4b}$$

$$\left[\overline{h}\right]\left[\overline{v}\right] = \frac{1}{N}\sum_{i=1}^{N}[h_i]\frac{1}{N}\sum_{i=1}^{N}\left[v_i\right], \tag{4c}$$

$$\overline{[h'][v']} = \frac{1}{N}\sum_{i=1}^{N}[h_i - \bar{h}]\left[v_i - \bar{v}\right], \tag{4d}$$

$$\left[\overline{h^* v^*}\right] = \frac{1}{N}\sum_{i=1}^{N}\left[\left(h_i - [h]_i\right)\left(v_i - [v]_i\right)\right]. \tag{4e}$$

The left-hand sides of Eqs. (4b), (4c), (4d), and (4e) are the total meridional transport of the h, meridional flux of h by the mean meridional circulation (or regional Hadley circulation), transient eddies (sub-seasonal or intraseasonal variations), and the standing eddies respectively. Here, v_i is the meridional wind for a given day (i) at a specific grid point and pressure level, N is the number of days in the JJAS season (= 120 days). The zonal brackets and the overbars represent zonal average from 60°E to 100°E and time mean over JJAS season respectively.

Since, we are dealing with a limited longitudinal domain (from 60°E to 100°E) east–west boundary flux ($\overline{B_Q}$) is non-zero and is estimated as:

$$\overline{B_Q} = \int_{p_{top}}^{p_{bot}}\left(\frac{1}{N}\sum_{i=1}^{N}\left\{h_i u_i\right\}_{100E} - \left\{h_i u_i\right\}_{60E}\right)\frac{dp}{g}, \tag{5}$$

where u_i is the zonal wind for a given day (i) at a specific grid point along either 100°E or 60°E longitude. Substituting Eq. (4a) in (3) we get:

$$\overline{\frac{\partial[H]}{\partial t}} = \underbrace{-\frac{\partial}{\partial y}\int_{p_{top}}^{p_{bot}}\left[\bar{h}\right]\left[\bar{v}\right]\frac{dp}{g}}_{} \underbrace{-\frac{\partial}{\partial y}\int_{p_{top}}^{p_{bot}}\overline{[h'][v']}\frac{dp}{g}}_{} \underbrace{-\frac{\partial}{\partial y}\int_{p_{top}}^{p_{bot}}\left[\overline{h^* v^*}\right]\frac{dp}{g}}_{} \underbrace{-\overline{B_Q}}_{} \underbrace{-\int_{p_{top}}^{p_{bot}}\frac{\partial\overline{[\omega][h]}}{\partial p}\frac{dp}{g}}_{} \underbrace{+\left[\overline{Q_R}\right]}_{} \underbrace{+\overline{[EF]}}_{}. \tag{6}$$

The terms on the right-hand side of Eq. (6), are computed from gridded ERA-Interim reanalysis (ERA-I; Dee et al. 2011) available at reduced Gaussian grid N128 from 1000 hPa ($=p_{bot}$) to 100 hPa ($=p_{top}$) at daily interval from 00z01 June through 00z30 September of each year. We compute all terms of Eq. (6) from 1985 through 2014. It may be noted that the first, second, and third terms on the right-hand side of Eq. (6) are the meridional flux transport of H by the regional Hadley cell, transient eddies and stationary eddies respectively.

In order to analyze the relative contributions of the terms in the right-hand side of Eq. (6) to the tendency of the seasonal mean H (left hand side of Eq. 6), we will follow Kang et al. (2001) to compute partial co-variance (PCOV) between two variables A and B as:

$$PCOV(A,B) = \frac{\frac{1}{N}\sum_{i=1}^{N}\left(A_i - \overline{A}\right)\left(B_i - \overline{B}\right)}{\sigma_A}. \tag{7}$$

The advantage of computing PCOV over say, correlation is that the latter simply shows the normalized linear relation between two variables (A and B) with no units while the former provides the actual magnitude of the variable B that is related to variable A. In our case, variable A is the time tendency of $\left[\overline{H}\right]$ in Eq. (6) and variable B will be the various terms on the right-hand side of Eq. (6). Furthermore, our interest here is not to compute a detailed budget of the H but to find the relative significance of the influence of the terms on the right-hand side of Eq. (6) to the tendency of H on seasonal time scales, which PCOV will sufficiently accomplish.

Like the budget equation of $\bar{H}$ in Eq. (1), the moisture budget equation is given as:

$$\frac{\partial\bar{Q}}{\partial t} = -\int_{p_{top}}^{p_{bot}}\nabla\cdot\overline{\vec{V}(q)}\frac{dp}{g} - \int_{p_{top}}^{p_{bot}}\frac{\partial\overline{\omega(q)}}{\partial p}\frac{dp}{g} - P + E, \tag{8}$$

where $Q = \int_{p_{top}}^{p_{bot}} q\frac{dp}{g}$, q is specific humidity, P and E are precipitation and surface evaporation respectively. One may infer from Eqs. (1) and (8) that a strong similarity exists in the behavior of MSE and Lq. Indeed, several studies (e.g. Kiranmayi and Maloney 2011; Adames and Ming 2018) have indicated that the variations in MSE on various spatial and temporal scales are mainly governed by moisture variations.

A strong positive correlation between column integrated moisture content and precipitation exist (e.g. Raymond 2000; Bretherton et al. 2004) and therefore increased horizontal convergence of specific humidity will likely lead to increased precipitation. Adames and Ming (2018) showed that a convergence of MSE, which is dominated by the convergence of moisture consequently leads to an increase in precipitation. This study analyses the moist static energy budget to understand the zonal mean precipitation variation.

3 Results

3.1 Zonal mean precipitation

As this study focusses on the zonal mean component of the seasonal precipitation (P) for June–July–August–September (JJAS) of the Indian summer monsoon. It makes sense

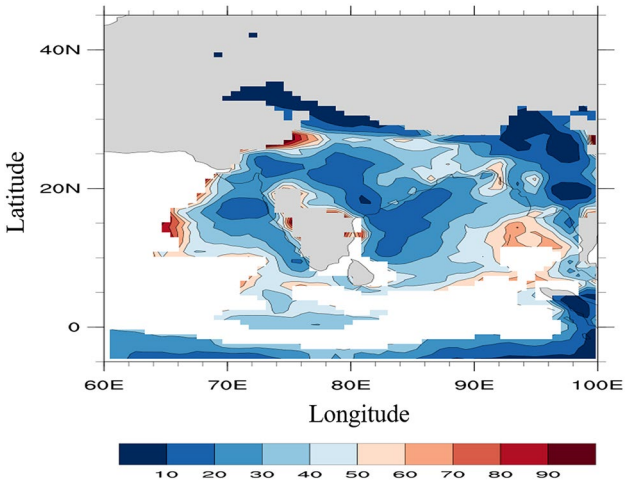

Fig. 1 The percent of the seasonal precipitation variation explained by the zonal mean component of the Indian summer monsoon. Regions with climatological seasonal mean JJAS rainfall variance below 2 mm^2 day^{-2} is masked out as grey over land and white over ocean

to first show the significance of zonal mean component. In other words, we start with the question: what fraction of the seasonal variation of the ISM precipitation is explained by the corresponding zonal mean component? The seasonal precipitation P could be divided it in two parts: horizontal mean (denoted by $[P]$) and perturbation (denoted by P'):

$$P = [P] + P'. \tag{9}$$

Now, if we apply the variance operator in time to calculate interannually variance in precipitation on both sides of Eq. 9, we get:

$$Var(P) = Var([P]) + Var(P'). \tag{10}$$

Therefore, the percentage of seasonal variation of ISM precipitation related to the variation of the corresponding zonal mean component is calculated as $\frac{Var([P])}{Var(P)} \times 100$ and is shown in Fig. 1. Figure 1 shows that the zonal mean precipitation of the ISM explains nearly 20–30% of the total seasonal mean precipitation of the ISM over the core monsoon region, which is quite significant.

The time-latitude cross-section of the zonal mean precipitation for JJAS indicates significant interannual variations (Fig. 2a). The largest temporal variations are

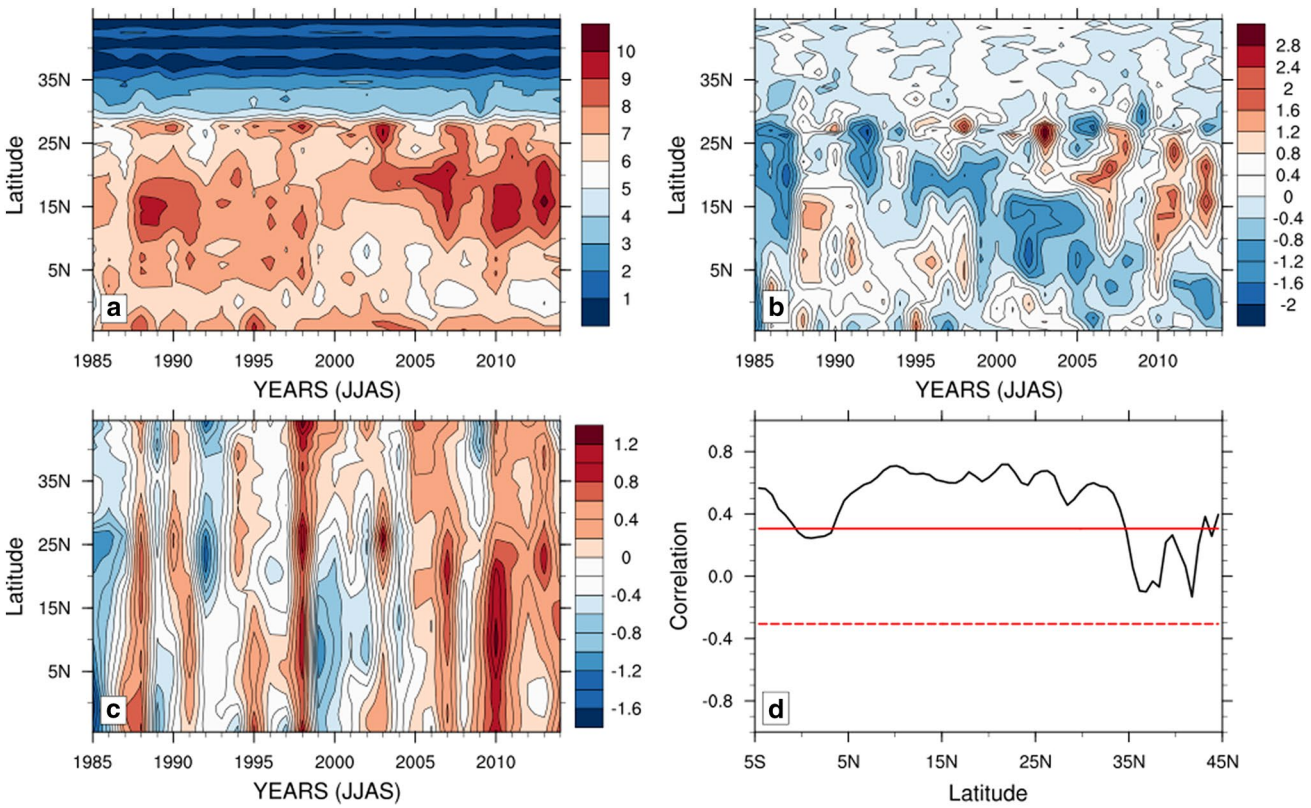

Fig. 2 Latitude-time cross-section of the zonal mean ISM **a** seasonal mean JJAS rainfall (mm day^{-1}), **b** seasonal mean JJAS rainfall anomalies (mm day^{-1}), **c** vertically integrated moist static energy anomalies (J m^{-2}), and **d** temporal correlation between ISM seasonal rainfall anomaly and vertically integrated moist static energy. The horizontal red lines in panel d correspond to the 90% significance level according to t test

bound approximately between latitudes of 10°N and 25°N. Incidentally, these latitudes coincide with the core of the ISM in central India (Goswami and Xavier 2003; Rajeevan et al. 2010). The interannual variations of the zonal mean JJAS precipitation anomalies (Fig. 2b) clearly indicate that ~ 10°N to 25°N latitudes bound some of the largest amplitudes (Fig. 2b). The corresponding zonal mean anomalies of H for JJAS (Fig. 2c) also shows significant interannual variations. Figure 2d shows that the correlations of the zonal mean precipitation anomalies of the ISM with the corresponding zonal mean anomalies of H are high including in the core latitude band of the ISM. The results in Figs. 1 and 2 suggest that the zonal mean framework could provide a viable avenue to understand ISM rainfall anomalies through the analysis of the zonal mean anomalies of H.

Figure 3a, b show the composite of the JJAS mean precipitation anomalies based on 5 years with maximum and minimum Z-scores (defined as the number of standard deviations a seasonal mean is from the climatological seasonal mean of 30 years i.e. $z_i = \frac{x_i - \bar{x}}{s}$, where $\bar{x}$ is sample mean and s is sample standard deviation) of the zonal mean precipitation JJAS anomaly averaged between 10°N and 25°N respectively. These composites demonstrate the relevance of the zonal mean JJAS precipitation anomalies of the ISM, as they correspond quite well with large scale seasonal anomalies of the ISM, at least for the most extreme seasons. The composite anomalies in Fig. 3a, b are similar to the ISM precipitation anomalies shown in Krishnamurthy and Shukla (2007). They indicate that the large-scale precipitation anomalies of the ISM over the Indian subcontinent is a combination of a seasonally persistent (and somewhat homogeneous precipitation anomaly) superposed with the residual spatially heterogeneous intraseasonal anomalies.

3.2 Time tendency of moist static energy

In Figs. 4 and 5 we show the PCOV of the various forcing terms in Eq. 6 with the time tendency of H. The meridional flux of H by the regional Hadley circulation (term 1 on the RHS of Eq. 6; Fig. 4a) dominates over all other forcing terms (Figs. 4b–d, 5a–c) in the contribution towards the tendency of H (LHS of Eq. 6) in the core latitude of the ISM (10°N–25°N). It may also be noted that the PCOV of the meridional flux of H by the regional Hadley cell is largely positive in Fig. 4a over this core monsoon latitude range. It suggests that with strengthening of the meridional flux of H by the regional Hadley cell the zonal mean tendency of H increases and vice versa. In the latitude range of 6°N–14°N the PCOV is negative, which suggests that it is the region of the descending branch of the regional Hadley cell. The transverse boundary flux of H (term 4 in the RHS of Eq. 6; Fig. 4d) and the vertical flux of h (term 5 in the RHS of Eq. 6; Fig. 5a) are the next biggest contributors to the tendency of H. Although both of these latter forcing terms are

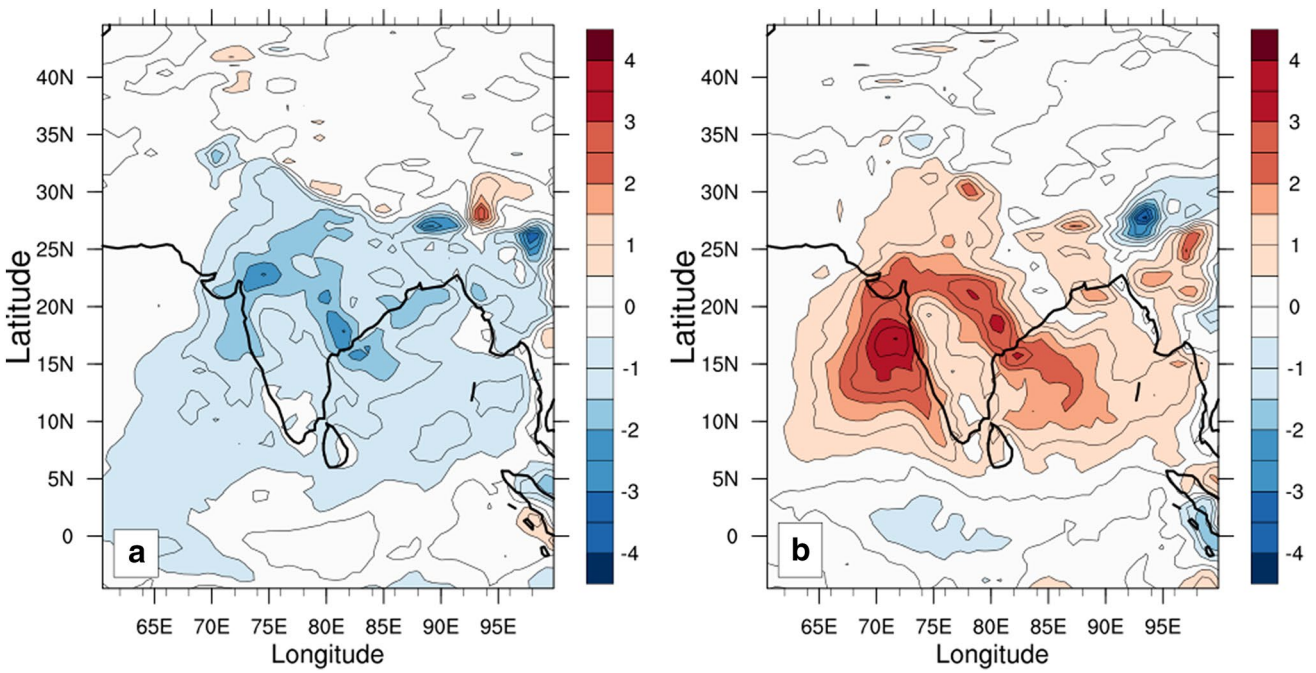

Fig. 3 The time latitude cross-section of the composited precipitation anomaly over 5 years with **a** maximum and **b** minimum five Z-scores of the zonal mean precipitation JJAS anomaly averaged between 10°N and 25°N. Units: mm day^{-1}

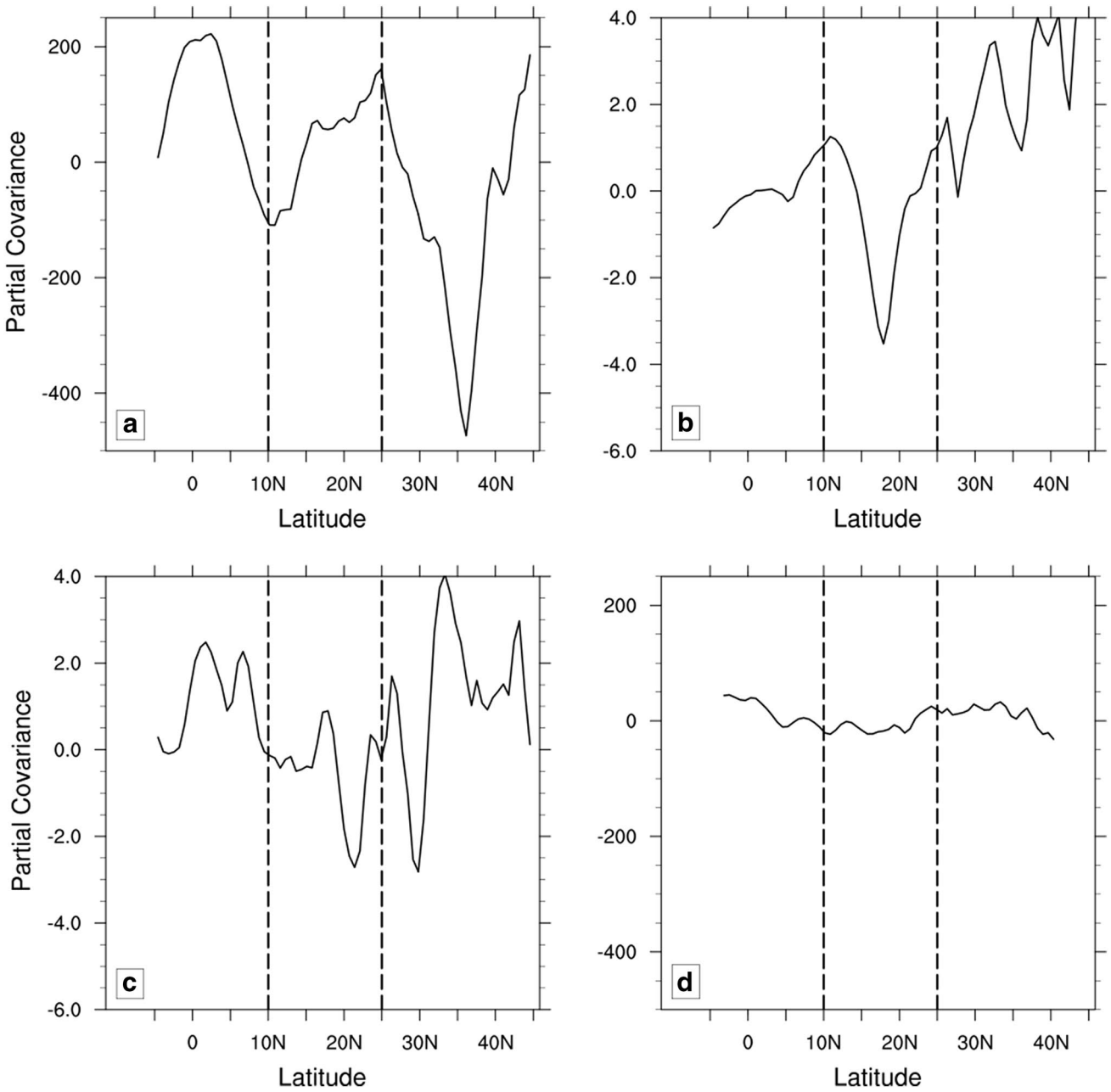

Fig. 4 The partial covariance (W m^{-2}) of meridional transport of H by **a** regional Hadley cell (term 1 of Eq. 6), **b** transient eddies (term 2 of Eq. 6), **c** standing eddies (term 3 of Eq. 6), and **d** boundary flux (term 4 of Eq. 6) with time tendency of H. The vertical dotted lines in the panels indicate the core latitudes of the ISM

in the same order of magnitude as the meridional flux of H by the regional Hadley cell, their magnitudes are significantly smaller in the core latitude of the ISM. The PCOV of the boundary flux of H with the zonal mean tendency of H in Fig. 4d is largely negative between ~ 10°N and 21°N and positive between 21°N and 25°N. Similarly, the PCOV of the vertical flux of h with the tendency of H in Fig. 5a is negative between ~ 10°N and 14°N and positive thereafter till 25°N. The sign of PCOV in Fig. 5a is consistent with the notion of the regional Hadley cell of the ISM. The regional Hadley cell has its rising branch over central India and the descending branch of the overturning circulation in the lower latitudes. Which would warrant the PCOV of the vertical flux of h with the zonal mean tendency of H to have a similar sign as displayed in Fig. 5a. The next set of forcing terms including the transport of H by transient eddies (term 2 in RHS of Eq. 6; Fig. 4b), standing eddies (term 3 in RHS of Eq. 6; Fig. 4c), radiative forcing (term 6 in the

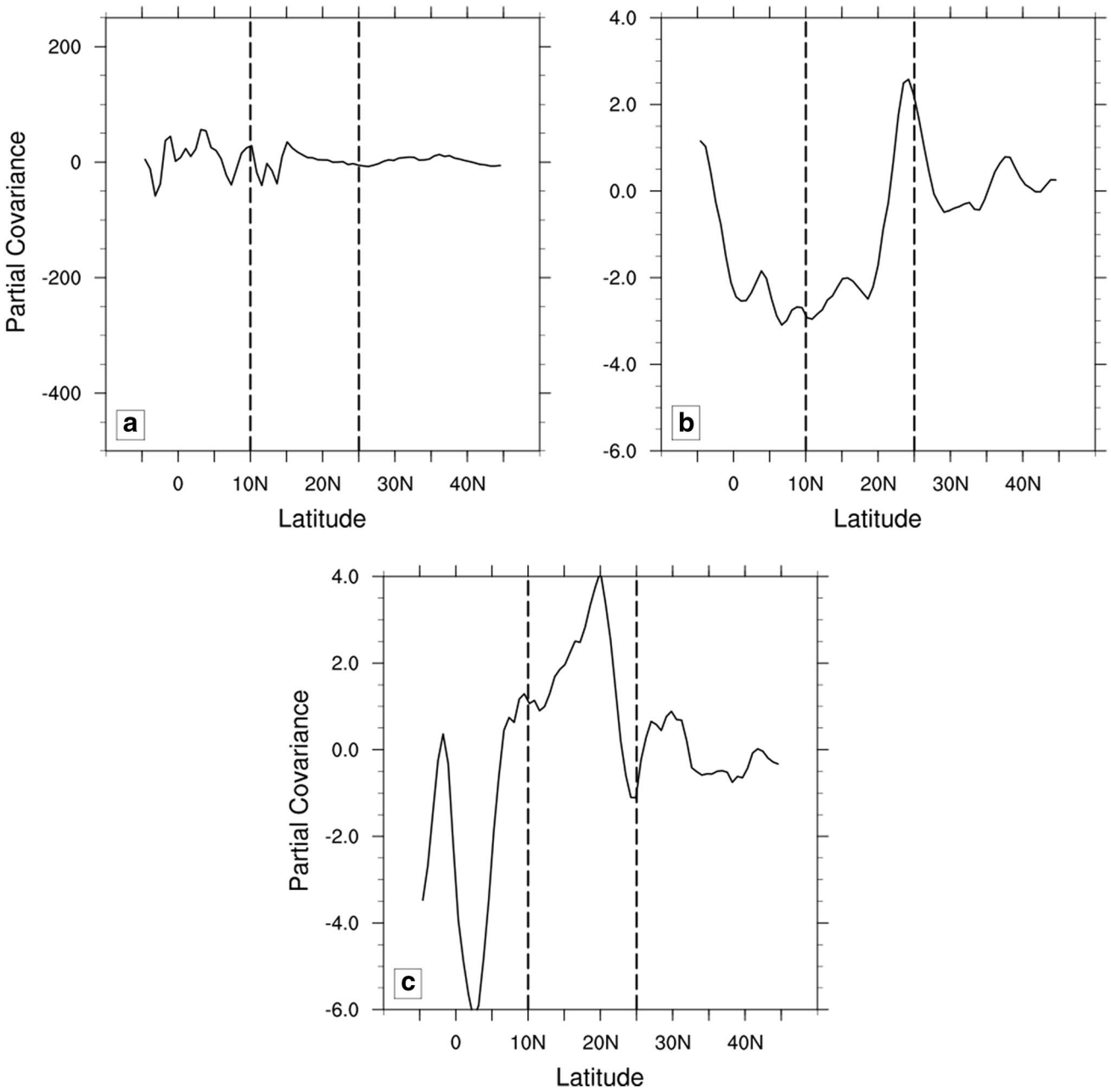

Fig. 5 The partial covariance (W m^{-2}) of **a** vertical flux of H (term 5 of Eq. 6), **b** radiative heating (term 6 of Eq. 6) and **c** enthalpy fluxes (term 7 of Eq. 6), with time tendency of H. The vertical dotted lines in the panels indicate the core latitudes of the ISM

RHS of Eq. 6; Fig. 5b), and enthalpy flux (term 7 in RHS of Eq. 6; Fig. 5c) are similar but at least an order of magnitude smaller than the previous three forcing terms (Figs. 4a, d, 5a). The transient (Fig. 4b), standing (Fig. 4c) eddies, and the radiative term (Fig. 5b) have a negative PCOV with the zonal mean tendency of H at interannual scales, which would suggest that these forcing terms are a weak deterrent forcing of H in the critical latitudes of the ISM. The PCOV of the radiative forcing (Fig. 5b) is negative in 10°N–20°N range and positive in the latitude range of 20°N–25°N. It could be again indicative of the contribution of the overturning circulation of the regional Hadley cell. Where the location of the rising branch is likely to produce net radiative heating in the column (on account of the prevalence of high level cirrus clouds) and the descending branch in the lower latitudes being relatively cloud free. Similar increases of column integrated radiative heating were found in the buildup of the active phase of the Madden–Julian Oscillation

in the Indian Ocean (Sobel et al. 2014) and in the Tropical Ocean and Global Atmosphere Coupled Ocean–Atmosphere Response Experiment (TOGA COARE; Johnson and Ciesielski 2000) as a result of increase in Cirrus clouds. The PCOV of the enthalpy fluxes with the time tendency of H is largely positive but relatively weak compared to the other dominant forcing terms (Fig. 5c).

3.3 Covariability with zonal mean precipitation

In Figs. 6a–d and 7a–c, we show the correlations of zonal mean precipitation of the ISM with all the forcing terms on the RHS of Eq. 6. It is interesting to note that the meridional flux of H by the regional Hadley cell (Fig. 6a) and the vertical flux of h (Fig. 7a) have some significant correlations within the critical latitudes of the ISM. All the other forcing terms except the enthalpy flux (Fig. 7c) and the radiative

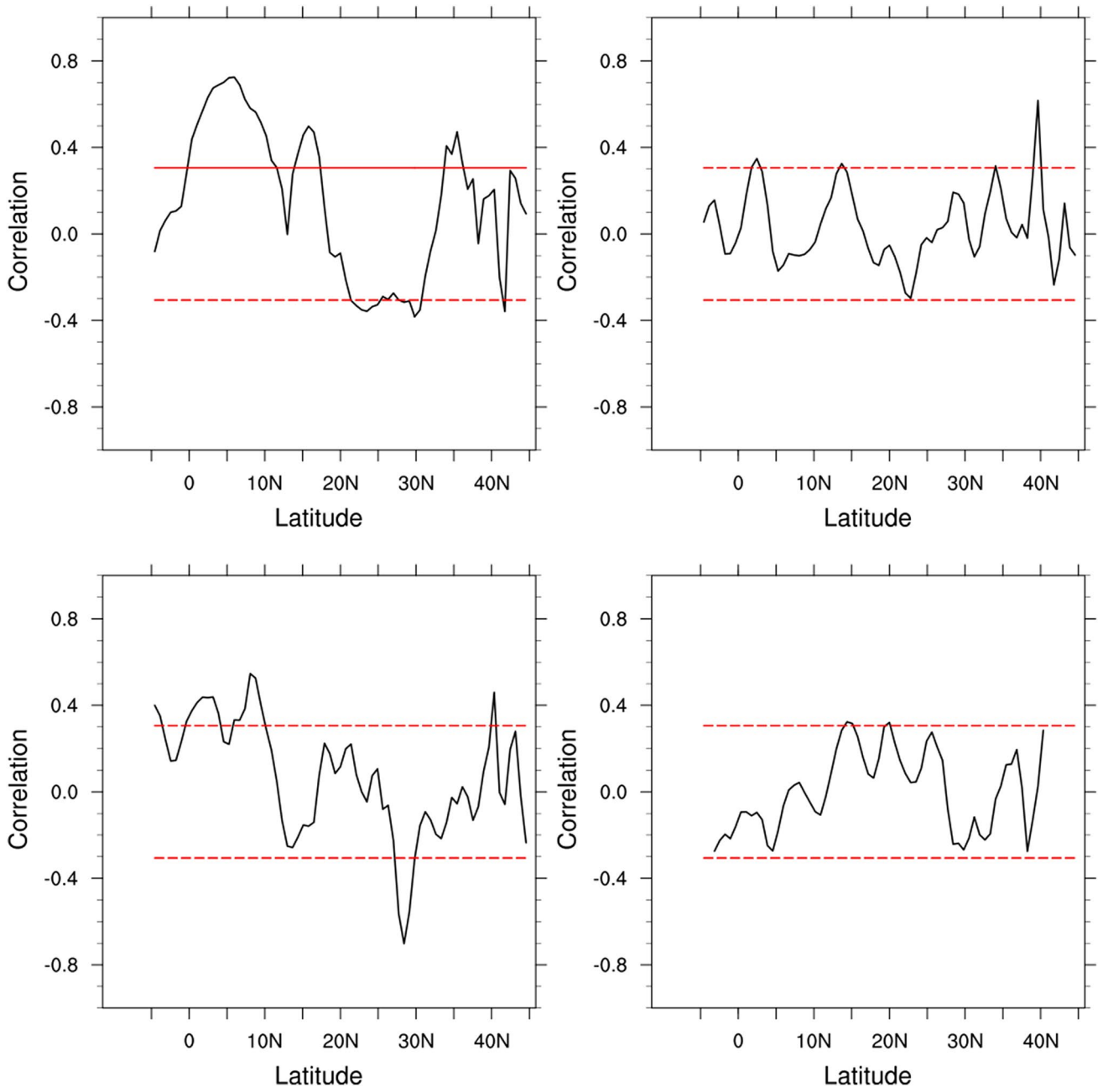

Fig. 6 The contemporaneous temporal correlation of seasonal mean JJAS and zonal mean precipitation of the ISM with meridional transport of H by **a** regional Hadley cell (term 1 of Eq. 6), **b** transient eddies (term 2 of Eq. 6), **c** standing eddies (term 3 of Eq. 6), and **d** boundary flux (term 4 of Eq. 6). The horizontal red lines correspond to 90% confidence interval according to t test

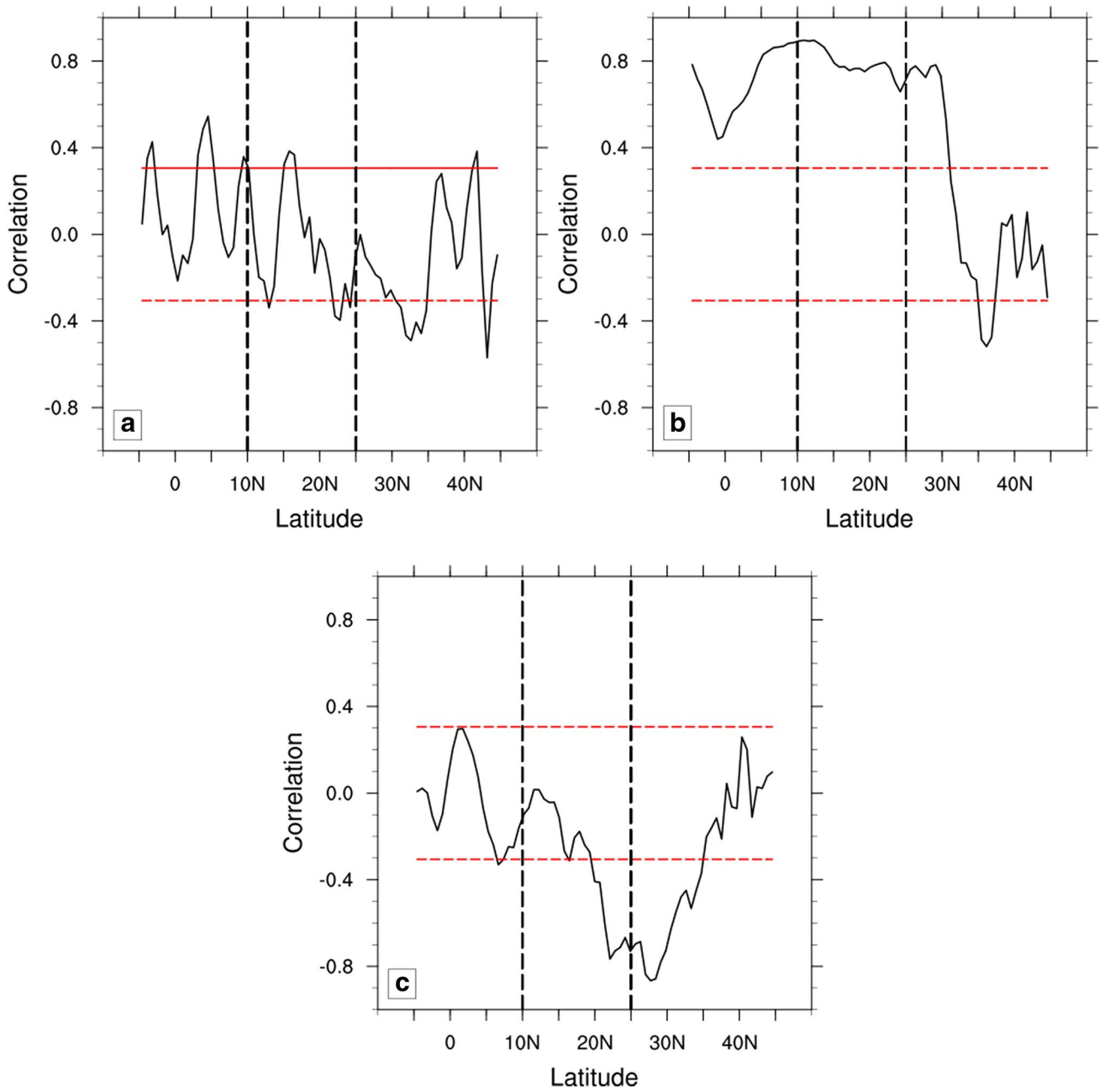

Fig. 7 The contemporaneous temporal correlation of JJAS seasonal mean and zonal mean precipitation of the ISM with **a** vertical flux of H (term 5 of Eq. 6), **b** radiative heating (term 6 of Eq. 6), and **c** enthalpy fluxes (term 7 of Eq. 6). The horizontal red lines correspond to 90% confidence interval according to t test

heating term (Fig. 7b) have insignificant correlations in the latitude range of ~ 10°N to 25°N with the zonal mean precipitation of the ISM. As noted earlier, the forcing terms of enthalpy flux and radiative heating are however, not some of the major contributors to the variability of H in ISM. These relationships shown in Figs. 6 and 7 illustrate the challenge in understanding the variations of the zonal mean precipitation of the ISM. These figures suggest that the forcing terms of H in total establish a robust relationship with the zonal mean precipitation anomalies (Fig. 2d) but the forcing terms of H individually relate very weakly with zonal mean rainfall except for the radiative flux and the enthalpy flux terms.

In Fig. 8a, b we show the difference of the composite zonal mean rain rate distribution for years with the most and the least Z-scores from the corresponding climatological distribution respectively. The composite difference for high and low Z-scores in Fig. 8c clearly shows that there is a greater frequency of 3–6 mm day^{-1} rain rates and lower

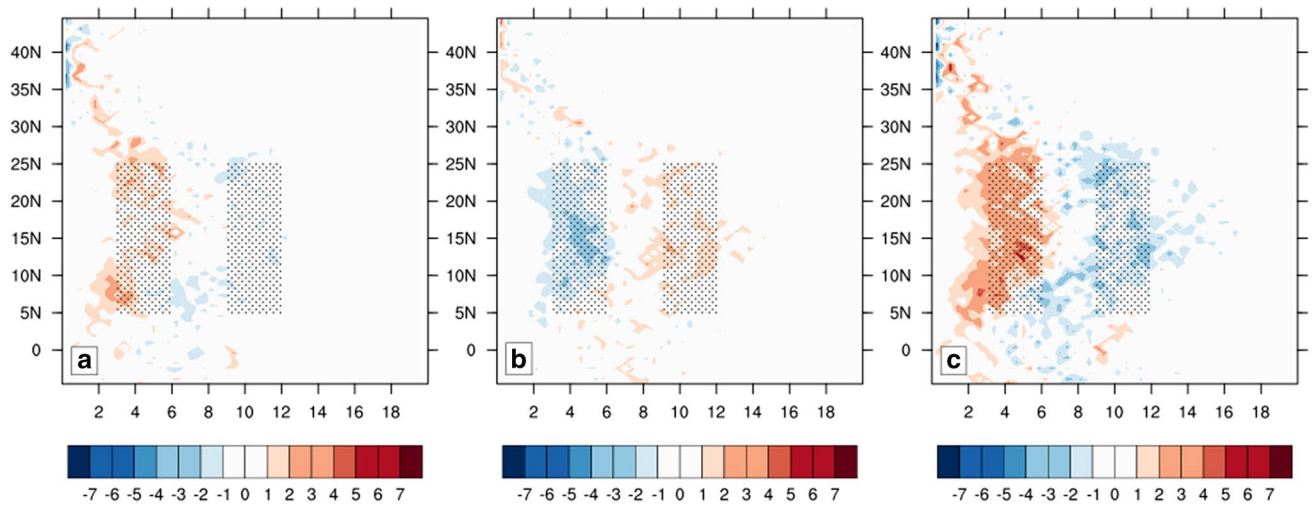

Fig. 8 The difference in the composite daily rain rate distribution of five JJAS seasons with **a** high, **b** low Z-scores from the corresponding daily climatological distribution for the JJAS season. **c** (**b**–**a**). The stippled regions in the panels show the rain rate ranges of 3–6 mm day^{-1} and 9–12 mm day^{-1} that exhibit the largest changes in these composites. The abscissa is rain rate with units of mm day^{-1}

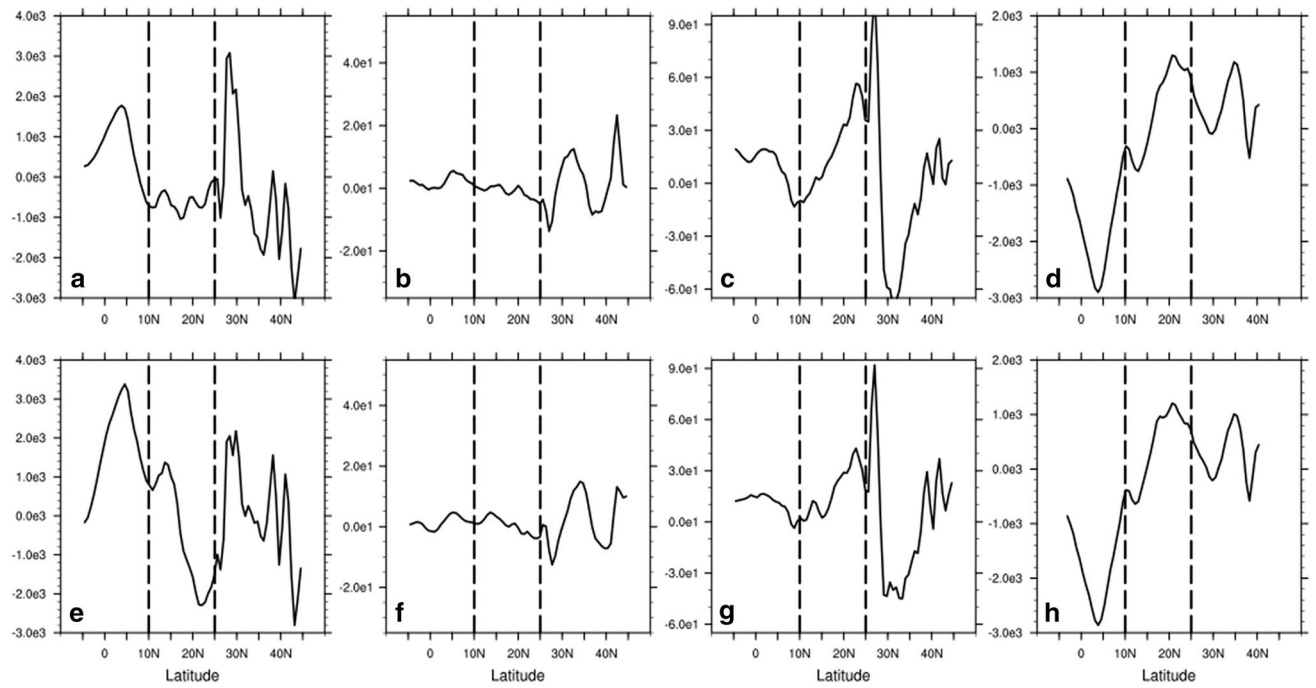

Fig. 9 Daily composites over the five ISM seasons with highest Z-scores taken at days when the rain rates were in the range of 3–6 mm day^{-1} (upper row; **a**–**d**) and lowest Z-score seasons when daily rain rates were in the range of 9–12 mm day^{-1} (lower row; **e**–**h**) for the right hand side terms (**a**, **e**) 1, (**b**, **f**) 2, (**c**, **g**) 3, and (**d**, **h**) 4 of Eq. 6. The units are in W m^{-2}

frequency of 9–12 mm day^{-1} in years with high Z-scores relative to years with low Z-scores. To examine these differences further, we composited the forcing terms of H for the days with these rain rates over the 10 isolated, extreme seasons in Figs. 9 and 10. Figure 9 shows that over the core monsoon region (10°N–25°N) the only significant difference in the forcing terms between the days with rain rates in the range between 3 and 6 mm day^{-1} in the highest Z scores years and the days with rain rate in the range between 9 and 12 mm day^{-1} in the lowest Z score is in the mean meridional

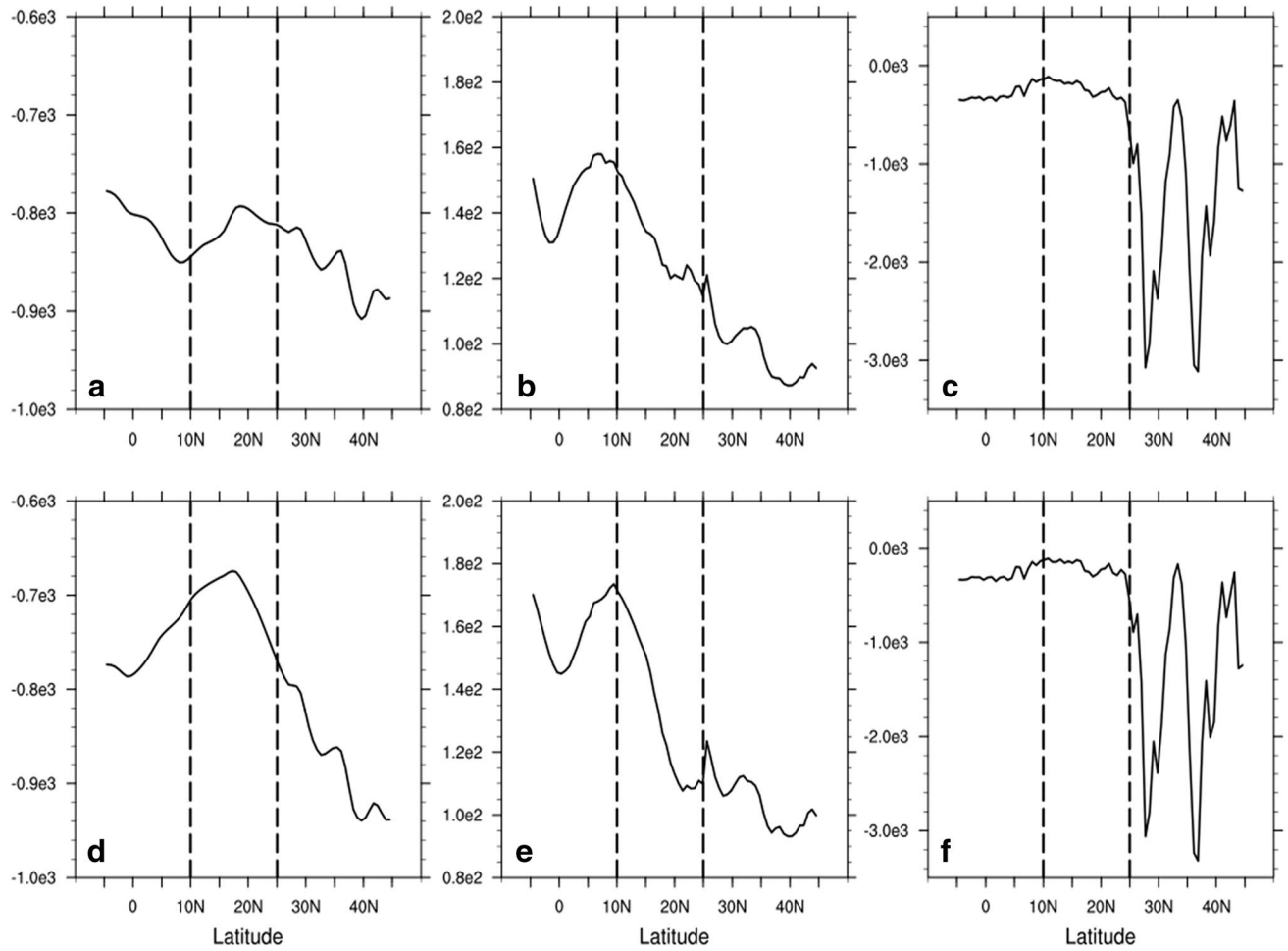

Fig. 10 Daily composites over the five ISM seasons with highest Z-scores taken at days when the rain rates were in the range of 3–6 mm day^{-1} (upper row; **a**–**c**) and lowest Z-score seasons when daily rain rates were in the range of 9–12 mm day^{-1} (lower row; **d**–**f**) for the right hand side terms (**a**, **d**) 6, (**b**, **e**) 7, and (**c**, **f**) 5 of Eq. 6. The units are in W m^{-2}

transport of MSE (term 1 in Eq. 6). In other words, Fig. 9a is suggestive of the variations of the regional Hadley cell with the variability of the rainfall. Additionally, Fig. 10 suggests that largely the radiative heating and up to some extent the surface enthalpy fluxes are responsible forcing terms differentiating the seasons with greater frequency of 3–6 mm day^{-1} rain rate days from seasons with lower frequency of 9–12 mm day^{-1}. Therefore, this alternative way of compositing the forcing terms highlights the important role of the meridional flux of H in determining the seasonal differences in ISM rainfall. This composite difference in Figs. 9 and 10 suggests that the extreme changes in rainfall in anomalous seasons are associated with changes in the strength of the regional Hadley cell. However, as indicated by the correlations in Figs. 6 and 7, the total zonal mean precipitation anomalies are weakly associated with any of the forcing terms of H but significantly related to the total corresponding changes in H (Fig. 2d).

4 Conclusions

Several earlier studies have reported the close association of the variations of the regional Hadley cell with the ISM seasonal rainfall. We therefore wanted to investigate the variations of the zonal mean precipitation of the ISM, as we believed that in this reduced dimensional space the role of the regional Hadley cell will be exaggerated. It is observed that the zonal mean precipitation anomalies explain about 20–30% of the total seasonal precipitation of the ISM. Moreover, the zonally symmetric component becomes prominent in extreme ISM seasons. Therefore, investigating the variations of the zonal mean precipitation of the ISM is relevant.

The zonal mean precipitation anomalies of the ISM are closely associated with corresponding anomalies of zonal mean vertically integrated moist static energy (H). Our analysis indicates that the meridional flux of H by the regional Hadley cell is by far the largest forcing term of H followed

by the boundary flux of H and the vertical flux of moist static energy (h). All other forcing terms of H have relatively much smaller influence on the variations of H.

We find that the zonal mean precipitation anomalies of the ISM are modestly related to meridional flux of H by the regional Hadley cell. However, this relationship is inadequate to understand the variations of the zonal mean precipitation anomalies of the ISM in terms of the variations of the regional Hadley cell. In other words, it is the total variation of zonal mean H that is more relatable to corresponding precipitation anomalies of the ISM than the individual forcing terms of H (e.g. the regional Hadley cell). Therefore, in order to predict or simulate the variations of the ISM zonal mean seasonal precipitation anomalies it would be pertinent to get all the forcing terms of time tendency of the zonal mean H as reasonably well predicted as possible irrespective of the magnitude of their contribution to H.

Acknowledgements This work was partially funded by National Science Foundation Grant 1606296. First author received support from Department of Science & Technology, India under INSPIRE Faculty scheme (DST/INSPIRE/04/2017/001997).

References

Adames AF, Ming Y (2018) Moisture and moist static energy budgets of south asian monsoon low pressure systems in GFDL AM4.0. J Atmos Sci 75:2107–2123. https://doi.org/10.1175/JAS-D-17-0309.1

Bretherton CS, Smolarkiewicz PK (1989) Gravity waves, compensating subsidence and detrainment around cumulus clouds. J Atmos Sci 46:740–759. https://doi.org/10.1175/1520-0469(1989)046,0740:GWCSAD.2.0.CO;2

Bretherton CS, Peters ME, Back LE (2004) Relationships between water vapor path and precipitation over the tropical oceans. J Climate 17:1517–1528

Dee DP et al (2011) The ERA-Interim reanalysis: configuration and performance of the data assimilation system. Q J R Meteorol Soc 137(656):553–597

Goswami BN (1994) Dynamical predictability of seasonal monsoon rainfall: problems and prospects. Proc Indian Natl Sci Acad 60:101–120

Goswami BN, Xavier PK (2003) Potential predictability and extended range prediction of Indian summer monsoon breaks. Geophys Res Lett 30(18):1966. https://doi.org/10.1029/2003GL017.810.2003

Goswami BN, Krishnamurthy V, Annamalai H (1999) A broad-scale circulation index for the interannual variability of the Indian summer monsoon. R Meteorol Soc 125:611–633

Hadley G (1735) Concerning the cause of the general trade-winds. Philos Trans 29:58–62

Held IM, Hou AY (1980) Nonlinear axially symmetric circulations in a nearly inviscid atmosphere. J Atmos Sci 37:515–533. https://doi.org/10.1175/1520-0469(1980)0372.0.CO;2

Inoue K, Back L (2015) Column-integrated moist static energy budget analysis on various time scales during TOGA COARE. J Atmos Sci 72:1856–1871

Johanson CM, Fu Q (2009) Hadley cell widening: model simulations versus observations. J Climate 22:2713–2725. https://doi.org/10.1175/2008JCLI2620.1

Johnson RH, Ciesielski PE (2000) Rainfall and radiative heating rates from TOGA COARE atmospheric budgets. J Atmos Sci 57:1497–1514. https://doi.org/10.1175/1520-0469(2000)057,1497:RARHRF.2.0.CO;2

Joseph PV (1978) Subtropical westerlies in relation to large scale failure of Indian summer monsoon. Indian J Meteorol Hydrol Geophys 29:412–418

Kang I-S, An I-S, Jin F-F (2001) A systematic approximation of the SST anomaly equation for ENSO. J Meteorol Soc Japan 79:1–10

Kiranmayi L, Maloney ED (2011) Intraseasonal moist static energy budget in reanalysis data. J Geophys Res 116:D21117. https://doi.org/10.1029/2011JD016031

Krishnamurthy V, Goswami BN (2000) Indian monsoon–ENSO relationship on interdecadal timescale. J Climate 13:579–595. https://doi.org/10.1175/1520-0442(2000)013%3c0579:IMEROI%3e2.0.CO;2

Krishnamurthy V, Shukla J (2000) Intraseasonal and interannual variability of rainfall over India. J Climate 13:4366–4377. https://doi.org/10.1175/1520-0442(2000)013%3c0001:IAIVOR%3e2.0.CO;2

Krishnamurthy V, Shukla J (2007) Intraseasonal and seasonally persisting patterns of Indian monsoon rainfall. J Climate 20:3–20. https://doi.org/10.1175/JCLI3981.1

Li J, Wang B (2016) How predictable is the anomaly pattern of the Indian summer rainfall? Climate Dyn. https://doi.org/10.1007/s00382-015-2735-6

Lorenz EN (1967) The nature and theory of the general circulation in the atmosphere. WMO Publ, p 218

Lu J, Vecchi GA, Reichler T (2007) Expansion of the Hadley cell under global warming. Geophys Res Lett 34:L06805. https://doi.org/10.1029/2006GL028443

Neelin JD, Held IM (1987) Modeling tropical convergence based on the moist static energy budget. Mon Weather Rev 115:3–12

Nigam S, Ruiz-Barradas A, Sengupta A (2018) Laboratory for experimental hydroclimate prediction. http://monsoon.umd.edu

Oort AH, Rasmusson EM (1970) On the annual variation of the monthly mean meridional circulation. Mon Weather Rev 98:423–442

Oort AH, Yienger JJ (1996) Observed interannual variability in the Hadley circulation and its connection to ENSO. J Climate 9:2751–2767

Palmen EH (1963) General circulation of the tropics. In: Proceedings of the symposium on tropical meteorology, Rotorua, November 1963, Wellington, pp 3–30

Palmen EH, Vuorela L (1963) On the mean meridional circulations in the northern hemisphere during the winter season. Q J Roy Meteorol Soc 89:131–138

Rajeevan M, Gadgil S, Bhate J (2010) Active and break spells of the Indian summer monsoon. J Earth Syst Sci 119:229–247

Raymond DJ (2000) Thermodynamic control of tropical rainfall. Q J R Meteorol Soc 126:889–898. https://doi.org/10.1002/qj.49712656406

Riehl H (1963) Stationary aspects of the tropical general circulation. Geofisica Internacional 3(3/4):53–68

Schulmann LI (1973) On the summer hemisphere Hadley cell. R Meteorol Soc 99:197–201

Slingo JM, Annamalai H (2000) 1997: the El Niño of the century and the response of the Indian summer monsoon. Mon Weather Rev 128:1778–1797

Sobel AH, Bretherton CS (2000) Modeling tropical precipitation in a single column. J Climate 13:4378–4392. https://doi.org/10.1175/1520-0442(2000)013,4378:MTPIAS.2.0.CO;2

Sobel A, Wang S, Kim D (2014) Moist static energy budget of the MJO during DYNAMO. J Atmos Sci 71:4276–4291

Tucker GB (1959) Mean meridional circulations in the atmosphere. Q J R Meteorol. Soc 85:209–224. https://doi.org/10.1002/qj.49708536504

Vuorela LA, Tuominen I (1964) On the mean zonal and meridional circulations and the flux of moisture in the northern hemisphere during the summer season. Pure Appl Geophys 57:167–180

Waliser DE, Shi Z, Lanzante JR, Oort AH (1999) The Hadley circulation: assessing NCEP/NCAR reanalysis and sparse in situ estimates. Climate Dyn 15:719–735

Wang B, Xiang BQ, Li J, Webster PJ, Rajeevan MN, Liu J, Ha KJ (2015) Rethinking Indian monsoon rainfall prediction in the context of recent global warming. Nat Commun 6:7154. https://doi.org/10.1038/ncomms8154

Waugh DW, Garfinkel CI, Polvani LM (2015) Drivers of the recent tropical expansion in the southern hemisphere: changing SSTs or ozone depletion? J Climate 28:6581–6586 **(in press)**

Webster PJ, Yang S (1992) Monsoon and Enso: selectively interactive systems. Q J R Meteorol Soc 118:877–926. https://doi.org/10.1002/qj.49711850705

Webster PJ, Magana VO, Palmer TN, Shukla J, Tomas RA, Yanai TM, Yasunari T (1998) Monsoons: processes, predictability, and the prospects for prediction. J Geophys Res 103:14451–14510

Yanai M, Esbensen S, Chu J (1973) Determination of bulk properties of tropical cloud clusters from large-scale heat and moisture budgets. J Atmos Sci 30:611–627. https://doi.org/10.1175/1520-0469(1973)030%3c0611:DOBPOT%3e2.0.CO;2

Yasunaga K, Mapes B (2012) Differences between more divergent and more rotational types of convectively coupled equatorial waves. Part I: space-time spectral analyses. J Atmos Sci 69:3–16. https://doi.org/10.1175/JAS-D-11-033.1